

Article

Evaluation of Ni-Cu Ore from Zapolyarnoe Based on Mineralogical and Physical Properties before and after Comminution

Arturo H. Bravo , Holger Lieberwirth and Oleg Popov

Institute of Mineral Processing Machines and Recycling Systems Technology, Technical University Bergakademie Freiberg (TUBAF), Lampadiusstrasse 4, 09599 Freiberg, Germany; holger.lieberwirth@iart.tu-freiberg.de (H.L.); oleg.popov@iart.tu-freiberg.de (O.P.)

* Correspondence: bravo@iart.tu-freiberg.de

Abstract: For the effective comminution and subsequent enrichment of mineral ores, comprehensive knowledge of their mineralogical and physical properties is required. Using an integrated methodology, this study evaluated samples of polymetallic Ni-Cu ore from Zapolyarnoe, Russia. Several analytical techniques were utilised, including optical microscopy, microindentation with Vickers geometry, the Point Load Test, and Mineral Liberation Analysis (MLA). The purpose of this study was to determine mineral associations, physical features, and enrichment during jaw crusher comminution. The acquired properties included the Point Load Strength Index, Vickers Hardness Number, and fracture toughness. The MLA method characterised seven fractions in terms of particle size distribution, degree of liberation, association, and modal mineralogy. Magnetite, pyrrhotite, pentlandite, and chalcopyrite were calculated in terms of wt% and their textural features. The enrichment of each ore phase in fractions with particle sizes smaller than 400 μm was determined. The influence of this enrichment was discovered to be correlated with various textural and structural parameters, such as intergrowth, grain size, and crack morphologies after indentations. In addition, the chromium content of magnetite contributed to an increase in the fracture toughness values. Despite the complexities involved, even limited samples of materials provide valuable insights into processing behaviour, emphasising the importance of considering mineralogical parameters in comminution studies.

Keywords: comminution; ore minerals; copper–nickel deposits; jaw crusher; Point Load Test; Mineral Liberation Analysis; vickers hardness; enrichment



Citation: Bravo, A.H.; Lieberwirth, H.; Popov, O. Evaluation of Ni-Cu Ore from Zapolyarnoe Based on Mineralogical and Physical Properties before and after Comminution. *Minerals* **2024**, *14*, 493. <https://doi.org/10.3390/min14050493>

Academic Editors: Ngonidzashe Chimwani and Murray M. Bwalya

Received: 19 March 2024

Revised: 23 April 2024

Accepted: 4 May 2024

Published: 7 May 2024



Copyright: © 2024 by the authors. Licensee MDPI, Basel, Switzerland. This article is an open access article distributed under the terms and conditions of the Creative Commons Attribution (CC BY) license (<https://creativecommons.org/licenses/by/4.0/>).

1. Introduction

Manufacturing has recently experienced an increase in the demand for mineral raw materials. To address this increase, the manufacturing has processed ores from less conventional mineral deposits and deposits of lower grades [1–4]. Low-grade ore processing requires new technologies and economic models. In particular, selecting adequate processing technologies is crucial for the economic and sustainable production of metals and non-metals, as the stage of ore processing influences the quality of the final product [5,6].

To process a material, valuable minerals must be liberated, especially considering that comminution is one of the most energy-intensive processes, typically accounting for 30 to 50% of the energy consumption in a mining operation [7]. The field of processing research has technologies for the development of advanced comminution, which have aimed to reduce energy consumption and advance more practical and reliable process models [8]. Still, comminution remains a field for further technological research. For example, obtaining the minimum breakage load for the liberation of valuable minerals, staged recovery, and progressive improvements are approaches that several researchers have targeted for a wide variety of industrial sectors [9–11], e.g., the tracing of minerals from exploration. Selective disintegration and pre-concentration in the crushing stage have collectively been identified as a fundamental approach when discussing comminution and

grinding processes [12]. In identifying important parameters for comminution, researchers have studied both the particle size reduction in the feed material as well as the liberation of valuable minerals from the gangue [13].

Selective comminution aims to take advantage of the varying breakage characteristics of minerals within an ore, resulting in liberation at comparably coarse particle sizes. This selectivity is also observed in natural processes, such as rock weathering. Despite some adaptation of processing methods to exploit mineral responses, there is currently no systematic approach to optimise processing for specific ores due to limited knowledge of response behaviours and the technological limitations of the available technologies [14].

Selective fragmentation often occurs at mineral interfaces when they are subjected to stresses beyond their tensile strength or by shear. This breakage mechanism is also known as intergranular breakage, as opposed to intragranular or preferential breakage, and occurs due to the strength differences of mineral grains. Several studies have discussed the dynamics of fragmentation after exposure to impacts or compressive stresses [15–22]. King [16] investigated preferential breakage in grinding and identified six distinct phenomena that occur between random fracture and detachment. These phenomena involve the selective breakage of intergranular and intragranular bonds, as well as the preferential comminution of mineral phases. More recently, it has been reported that breakage is influenced by mineral properties such as hardness, cleavage, and grain size [23–27]. Those studies have discussed the dynamics of fragmentation after exposure to impact or compressive stresses and the importance of the distinction between random and non-random breakage. It is observed that breakage, generated by external forces, is associated with zones of weakness and depends significantly on the intrinsic properties (e.g., shape, size, and strength) of the mineral phases constituting the rock, and non-random breakage has a significant impact on the particle size distribution and liberation characteristics. Thus, comprehending the behaviour of minerals and the nature of their boundaries is crucial in determining the success of the process of comminution. Typically, in the early stages of designing the mineral processing facilities for a new mine, only a small amount of sample material is available, usually from drill cores. This research shows that even from such a small amount of sample material quite comprehensive information on processing behaviour can be drawn, even for such complex questions as selectivity in comminution.

This research assessed the relationship between mineralogical and physical properties and the results of selective comminution in crushing using copper–nickel samples from Zapolyarnoe, one of Russia’s largest polymetallic deposits. Zapolyarnoe is part of the Norilsk deposit, which is known for its significant concentrations of platinum group elements (PGEs) [28] and is located on the north-western edge of the Siberian platform in the Russian Arctic and hosts massive amounts of Ni-Cu ore [29]. The geodynamic conditions of this area were controlled by rifting and re-activation of the intra-continental basins [30]. Some authors describe an association with Permian–Triassic flood basalts and intrusion by basaltic magma during the Lower Permian–Triassic, forming a series of gabbroic rocks and leucocratic gabbro of the upper gabbro series of Norilsk deposits [28]. The classical model for Ni-Cu-PGEs states that mineralisation in this area is localised in the Norilsk–Kharaelakh valley and the northwestern flank of the Tunguska flood, with differentiated mafic-ultramafic intrusions along synclines [31–33].

The investigation included the characterisation of the material via optical microscopy of representative samples of both thin and polished sections. Using microindentation Vickers Hardness testing, the microhardness properties were determined for all mineral phases. The material underwent processing at the facilities of the Institute for Minerals Processing Machines and Recycling Systems Technology (IART), located at Technische Universität Bergakademie Freiberg, utilising a jaw crusher. Sub-samples of seven size fractions were subsequently subjected to Mineral Liberation Analysis (MLA) to ascertain the distribution of particle sizes, modal mineralogy, associations, and liberation of minerals. Selectivity and enrichment should at least be investigated in terms of their technical feasibility, focusing on the chalcopyrite, pentlandite, pyrrhotite, and magnetite phases. An integrated evaluation

of the physical and mineralogical properties obtained by the Point Load Test, Vickers microindentation, and detailed descriptions of the mineralogy under the microscope was considered appropriate to assess the selective comminution linked to the outcome.

During the investigation, the following questions were discussed:

- Is it possible, based on textural information obtained via optical microscopy, to identify certain mineralogical patterns that can provide valuable information for predicting the liberation of mineral phases of interest?
- Do the strength properties of the rock minerals (olivine and feldspar) and the ore phases differ sufficiently such that pentlandite, chalcopyrite, or pyrrhotite can be stressed by using suitable comminution processes so that the material can be broken down into different particle size classes via preferential breakage to subsequently allow separation with minimal loss of valuable material?
- Is it possible to show patterns in grain boundaries and their behaviour, such as a qualitative observation of interfacial fracture formation or preferential breakage? How does this relate to the observed mineralogical characteristics?
- What can be concluded regarding the data obtained via MLA and the fractions generated with compression stress using jaw crushers?

2. Materials and Methods

2.1. Materials

Ni-Cu Drill core samples were collected from the Zapolyarnoe deposit (Figure 1a). The combined drill cores had a total starting mass of 2 kg. Following a macroscopic observation after obtaining a fresh surface, two samples are selected, from each of which three polished sections and three thin sections that are oriented orthogonally were prepared (Figure 1b,c). This assessment enabled the acquisition of relevant and representative information concerning the material received from St. Petersburg Mining University, despite limited details regarding the location and spatial variation of samples. The drill cores have an inside diameter ranging from 35 mm (mostly) to 48 mm. The samples were evaluated together because, after investigation under a microscope, no significant differences were found in the samples.

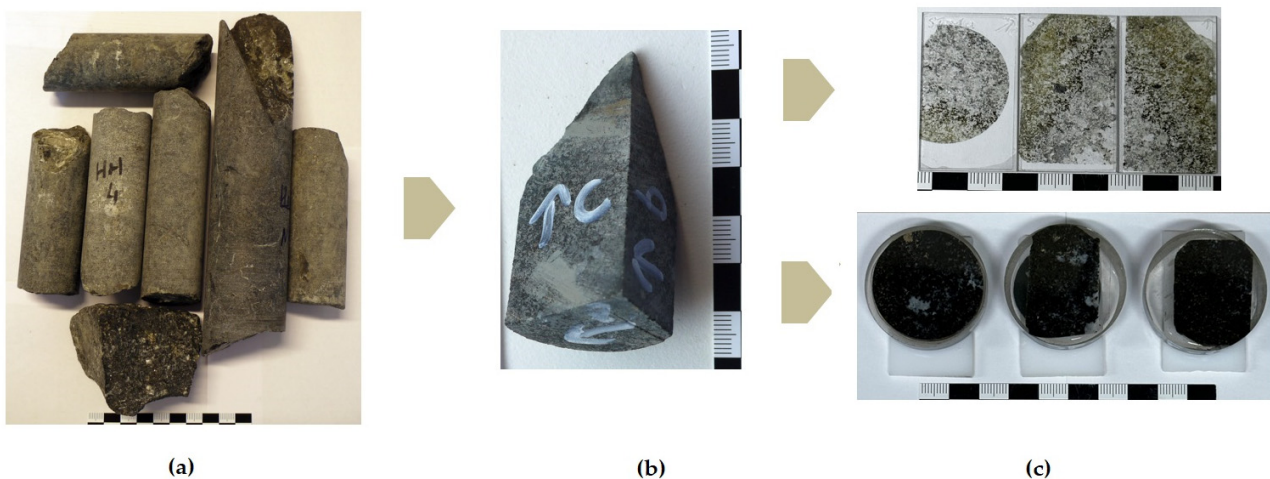


Figure 1. Zapolyarnoe Ni-Cu drill cores. (a) Drill core collected from Zapolyarnoe. (b) One of the selected samples with orientation marks and (c) the respective set of thin and polished sections.

2.2. Methods

The Ni-Cu ore material was characterised using various methods, starting with the determination of the strength index using the Point Load Test (PLT). Once the representative samples were selected, the assays were prepared as described in the following flow chart (Figure 2).

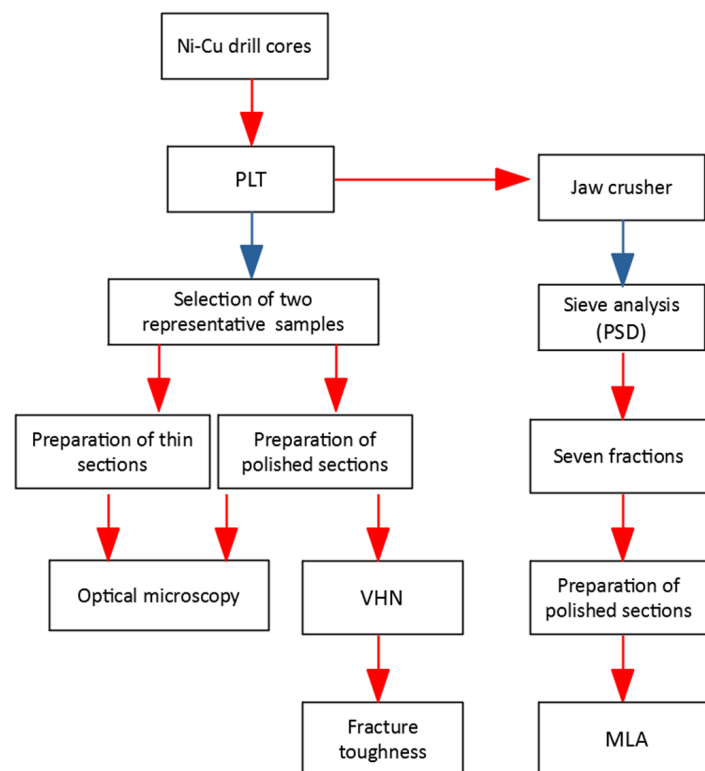


Figure 2. Flowchart of investigations. PLT: Point Load Test. VHN: Vickers Hardness Number. MLA: Mineral Liberation Analysis. PSD: particle size distribution.

2.2.1. Point Load Test

The Point Load Test (PLT) is employed for rock strength classification [34–37]. A notable advantage of this procedure in comparison to other methods (e.g., the Brazilian Test and uniaxial compressive strength) is its limited requirements for the preparation of rock specimens. The test can be conducted quickly and simply with a portable tester either at a quarry or in a laboratory (e.g., Point Load Tester (manufacturer: WILLE Geotechnik)). Fragments of drill cores are sufficient for this method.

The application of a specific load on a rock specimen until breakage occurs defines the strength index (I_s) and can be used for the classification or characterisation of rock samples. The I_s can be calculated from the load on the fracture [36], the platen tip spacing, and the width of the fracture surface (Figure 3). This can be obtained from Equation (1a) using the breaking load (P) (in kN) and the equivalent core diameter (D_e) (in mm), which is obtained from Equation (1b) using the minimum cross-sectional area (A) of the blocky sample. This area is calculated from the distance (D) (in mm) between the contact points and the narrower dimension width W (in mm) of the blocky sample, as in Equation (1c). The incorporation of the equivalent diameter (D_e) is useful to compare results from irregularly shaped specimens with diametral results (Figure 3).

$$I_s = \frac{P}{D_e^2} \quad (1a)$$

$$D_e^2 = 4 \frac{A}{\pi} \quad (1b)$$

$$A = WD \quad (1c)$$

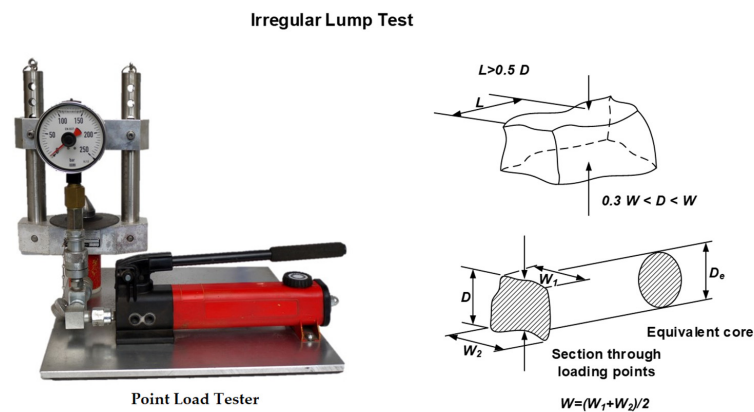


Figure 3. Point Load Tester used (left) with the measurement for irregularly shaped specimens [36].

The I_s depends greatly on the total size of the specimen. This effect, which is also seen with all other procedures (e.g., the uniaxial compression test), is generally referred to in rock mechanics as the scale effect [38]. Since the specimen size influences the strength index, the strength indices of rock pieces of different dimensions must be converted into values for a standard specimen with a standard diameter ($D_e = 50$ mm) to allow the comparison of results. The strength thereby changes to the $I_{S(50)}$. Broch [34] used an idealised set of curves that should enable the reduction in every individual value for the I_s arbitrary distance (D) to a standard value $I_{S(50)}$. For the possible regression of measurement data on a logarithmic grid [34,36], the I_s specifies a grain size correction factor (f), which enables conversion to the $I_{S(50)}$ for rocks (Equation (2)). In the equation, m is equal to the regression curve's gradient constant.

$$I_{s(50)} = f \cdot \frac{P}{D_e^2} = \frac{P}{D_e^2} \cdot \left(\frac{D_e}{50} \right)^{2(1-m)} \quad (2)$$

The strength index was determined using a test instrument from WILLE. The measurement range of this instrument is between 0 and 400 bar. The Point Load Test could be carried out on irregularly shaped particles as well as core samples. The calculation of point load indices (I_s) was performed following the guidelines of ISRM [36]. The $I_{S(50)}$ values were determined according to Raaz [39].

Given the presence of an empirical correlation between the Uniaxial Compressive Strength (UCS) and the Point Load Index ($I_{S(50)}$), it is possible to approximate the order of magnitude of the UCS by multiplying the $I_{S(50)}$ value by a conversion factor (Equation (3)) that requires specific determination for a given ore [40,41]. The relationship between the strength index ($I_{S(50)}$) and the compressive strength (σ_D) as a constant has been described by many researchers [35,37]. The ISRM [36] suggests indicating a relationship for the σ_D and the $I_{S(50)}$ of 20 to 25. On the basis of extensive Point Load tests conducted at the IART, the conversion factor can be defined as $c = 25$.

$$\sigma_D = c \cdot I_{S(50)} \quad (3)$$

With the limited amounts of sample materials from drill cores, a statistically substantiated result often cannot be obtained, but it is always possible to conduct assays and draw conclusions about the variance in the results. However, quarter and half drill cores, which are often available for the investigations described here, are not sufficient to process regular samples.

For the UCS test, the dimensions still fit for Point Load tests. Furthermore, it helps in the selection of representative samples for subsequent microindentation with Vickers geometry and MLA tests.

2.2.2. Optical Microscopy

Thin and polished sections were prepared after the PLT for a detailed investigation of mineralogical features. The representative samples were examined under an optical

microscope with transmitted and reflected light to describe and determine mineralogical data (mineral phases and alterations) and grain boundaries between the different mineral phases. Microscopic analysis was conducted using Zeiss Jena Jenapol (ZEISS, White Plains, NY, USA) and Olympus BX53M polarised-light microscopes equipped with JVC KY-F50 and Olympus U-TV1XC (Olympus, Tokyo, Japan) high-resolution digital cameras, respectively. This analytical method provided a way to identify with a relatively high resolution the phases within the textural framework.

2.2.3. Vickers Hardness Number and Fracture Toughness

While the PLT provides information on macroscopic features such as rock/ore strength, information on the behaviour of the valuable constituents has to be derived from the microscopic properties of the material constituents, the mineral grains, and the grain boundaries. The size of an indentation usually does not exceed 30 μm and this falls well within the size of many mineral grains. Even if a crack propagates towards or along a grain boundary, this may provide valuable information for comminution. The VHN test is seen as a promising approach to obtaining this information, and the morphology of the indentation can be classified.

The hardness of a material is generally expressed in terms of its resistance to local deformation. For its determination, tests based on the material's resistance to indentation are carried out. An indenter is pressed into the surface of the material with a known load. Then, the size of the subsequent indentation is measured: soft materials give a large indentation, and hard materials give a small one. To determine the VHN according to ISO6507 [42], a pyramidal indenter was pressed with an interface angle of 136° on a specimen with a defined test force. For the determination of fracture toughness, the propagation of cracks was considered [42,43]. L_1 , L_2 , L_3 , and L_4 are the lengths of radial cracks originating from four different edges of a Vickers indentation. An ideal case is $C_1 = a_1 + L_1$, $C_2 = a_2 + L_2$, $C_3 = a_3 + L_3$, or $C_4 = a_4 + L_4$ (Figure 4).

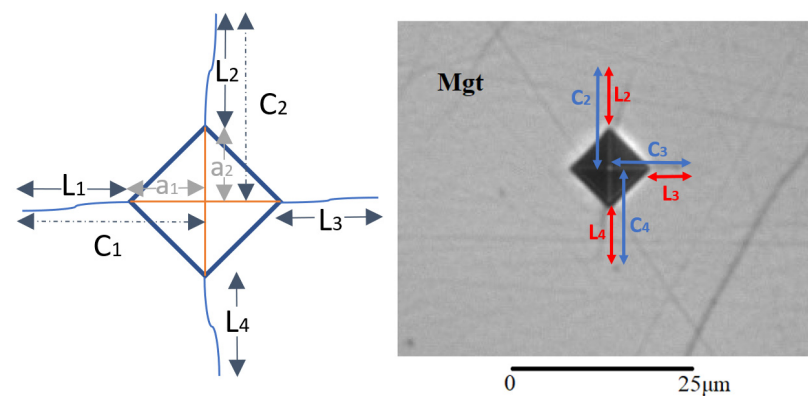


Figure 4. Example of fracture propagation evaluation in magnetite (Mgt). L_1 , L_2 , L_3 , and L_4 are the lengths of the radial cracks.

The Vickers Hardness results from the quotient of the applied test force (F in Newtons (N)) and the surface area of the residual indentation mark on the specimen. To calculate the surface area of the residual pyramidal indentation, the average of the two diagonals (d_1 and d_2 in mm) is used (Equation (4)) because the base areas of Vickers indents are frequently not exactly square (Figure 4). The recommended Vickers Hardness range is given in the standard ISO6507 [42].

$$HV = \frac{F}{A} = 2F \cdot \frac{\sin 68^\circ}{d^2} = \frac{1.8544 \cdot F}{d^2} \quad (4)$$

The crack lengths C_1 – C_4 that develop mainly at the corners of the indentation can be used to qualitatively and quantitatively characterise the fracture toughness (Figure 4).

Fracture toughness is measured to account for resistance to crack propagation. Theoretical models for estimating fracture toughness (K_{IC}) fracture toughness are based on a fracture mechanics approach. Previous research has investigated different ways of calculating the mechanical properties corresponding to radial–median cracks and the Palmqvist crack system [44,45]. This investigation considered the model of Blumenauer [46] (Equation (5)) giving values very similar (Equation (6)) [47] to the model of Tanaka [48] (Equation (7)).

$$K_{IC} = \frac{F_i}{(\pi \cdot c_n)^{\frac{3}{2}} \cdot \tan\left(\frac{\alpha}{2}\right)} \quad (5)$$

$$K_{IC} = 0.0726 \cdot \frac{F}{C^{\frac{3}{2}}} \quad (6)$$

$$K_{IC} = 0.0725 \cdot \frac{F}{C^{\frac{3}{2}}} \quad (7)$$

The investigation of the hardness and fracture toughness of different mineral phases via Vickers Hardness testing was carried out using the Shimadzu HMV-G21DT Micro Vickers Hardness tester. To provide a simplified description of the indentation morphologies, this study classified the results into five groups (Figure 5).

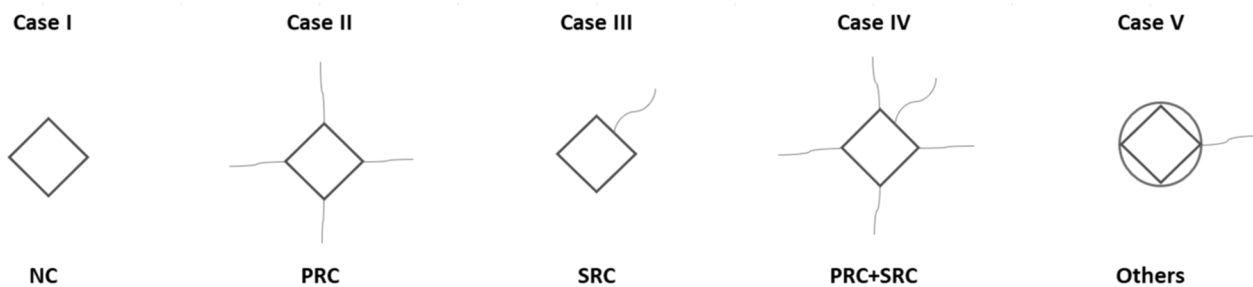


Figure 5. Morphology classification after indentations according to the most typical cases for this study. NC: no cracks; PRC: primary radial crack (which may have one, two, three, or four radial cracks (RCs)); SRC: secondary radial crack (which may have one, two, three, or four radial cracks (RCs)). Case IV includes all possible scenarios where primary and secondary radial cracks occur together. Additionally, case V encompasses other morphologies such as cone cracks or other irregular morphologies that cannot be classified in the previous categories.

The classification considers the formation of primary radial cracks (PRCs) and secondary radial cracks (SRCs), representing case II and case III, respectively. Primary radial cracks have an origin that lies in structures that are initiated after the indentation, and these cracks extend outward from the indentation site towards the edges. Subsequently, secondary radial cracks are mainly formed after primary cracks and propagate around them. The classification also includes cases where primary and secondary radial cracks are combined (case IV) and other types of cracks (case V) that may occur (e.g., if radial cracks are generated). If no cracks (NC) are observed after indentation, it is considered case I (Figure 5).

2.2.4. Mineral Liberation Analysis (MLA)

MLA can provide information on the particle shape and particle size distribution of smaller progenies and their modal mineralogy, mineral associations, and liberation. It is an important tool to evaluate the result of a comminution process, for instance with regard to selectivity. MLA combines an automated Scanning Electron Microscope (SEM) with multiple energy-dispersive X-ray detectors (EDS) to automatically acquire and jointly analyse images and elemental spectral information. SEM analysis of the samples enables automated analyses based on the evaluation of backscattered electron (BSE) images and the acquisition of energy-dispersive X-ray spectra of particles visible in the BSE imaging mode [49–51].

MLA analysis of Ni-Cu ore samples was performed at the Geometallurgy Laboratory, Institute of Mineralogy, TUBAF, using a scanning electron microscope FEI quanta 600 FEG (FEI, Hillsboro, OR, USA) equipped with a field emission source, two Bruker energy dispersive X-ray (EDX) SDD detectors, Bruker Quantax 200 with two Dual Xflash 5030 EDX detectors (Bruker, Berlin, Germany) and backscattered electron (BSE). The greyscale of the BSE image was calibrated with epoxy resin as the background (BSE grey level) and gold (pin in RDI standard block) as the upper limit (BSE grey level of about 250). The EDS X-ray spectrometers were calibrated with copper (pin in the RDI standard block). Several measurement modes are available in the MLA expert software, each calibrated for specific applications. In this study, the measurement mode GXMAP, i.e., grain X-ray mapping, was used. GXMAP uses X-ray mapping to identify phases that cannot be segmented using BSE grey levels alone. The Ni-Cu ore, which was previously crushed and divided into seven fractions, was analysed using MLA 2.9 software package (JKTech, Brisbane, Australia). For this purpose, the samples were embedded in epoxy resin. The ground surfaces of the resulting sections were coated with carbon and examined via SEM-EDS to identify the chemical composition and texture of the samples.

The mineral locking and degree of liberation data for each phase were obtained through MLA analysis. The mineral locking serves as an indicator to determine if a phase of interest is liberated or associated solely with another. The degree of liberation indicates the percentage of the ore's total content that consists of mineral particles that are not bound [52]. It is possible to represent and calculate it in one of the following ways:

Surface area: Liberation of a particle, expressed as a percentage, denotes the length fraction on the outer perimeter occupied by the mineral or minerals of interest in relation to the entire outer perimeter of the particle.

Volume: The area fraction of the mineral or minerals of interest in relation to the total area of the particle, typically expressed as a percentage, is denoted by the volume of liberation of the particle.

The degree of liberation of a mineral is frequently calculated in process mineralogy through the examination of two-dimensional sections of a particle set that is statistically representative and contains the mineral of interest. It is usually assessed based on the area percentage of the mineral grain(s) within a particle. Particles are often categorised into various grades based on incremental steps, such as 10% increments (100% liberated, 90–100% liberated, 80–90% liberated, etc.), or broader 30% steps such as <30% (locked), 30–60% (middlings), and >60% (liberated).

3. Results

3.1. Description of Optical Microscopy

Concerning the characteristics of the Zapolyarnoe samples, different mineral phases and relationships between them were identified and described. The results for rock-forming minerals and ore mineral phases are detailed in this section. The textural and structural information obtained is crucial for understanding and improving the size reduction process, mainly with respect to liberation size.

More than ten minerals were identified, mainly of mafic and calcium-rich phases such as olivine, mica (biotitic), and feldspar.

The ore was mainly composed of magnetite, pyrrhotite, pentlandite, and chalcopyrite with accessory amounts of ilmenite. Magnetite is the most abundant primary mineral of the ore and was mainly distributed in contact with olivine, pyrrhotite, ilmenite, and chalcopyrite (Figure 6d–f). Magnetite crystals were generally smaller than 0.4 mm (Figure 6e,f). Pyrrhotite generally occurred as anhedral grains. Grains with 1–2 mm diameters were commonly fractured and contained small euhedral to subhedral pyrrhotite crystals (Figure 6a). Pentlandite occurred as grains of various sizes enclosed within pyrrhotite and chalcopyrite. Pentlandite showed cataclastic fractures infilled with chalcopyrite and pyrrhotite (Figure 6b). Solid-state exsolution may occur when certain high-temperature minerals undergo cooling. In the case of pentlandite, a typical flame-like exsolution was observed

in pyrrhotite (Figure 6c). The paragenesis between pentlandite and pyrrhotite occurred in intergrowth between them and was disseminated throughout the sample. Chalcopyrite was also found along the edges of the intergrowth (Figure 6b,c). Ore minerals filled the interstices between crystals of pyroxene, olivine, and feldspar (mainly plagioclase). This means that the copper and nickel sources occurred later relative to the main rock-forming minerals. As for the main phases of the sample, olivine appeared to be the most common phase. Olivine was observed in relics of rhombic crystals (Figure 6d,g,i). Poikilitic pyroxene crystals with rounded olivine inclusions (Figure 6e) and plagioclase laths (Figure 6i) with polysynthetic twins were observed. Locally, the pyroxene formed subidiomorphic and elongated prismatic crystals measuring 1–2 mm (Figure 6h). Brown ferruginous biotite had short laminar and tabular forms ranging from 0.2 to 0.5 mm (Figure 6h) and locally it was possible to identify chlorite.

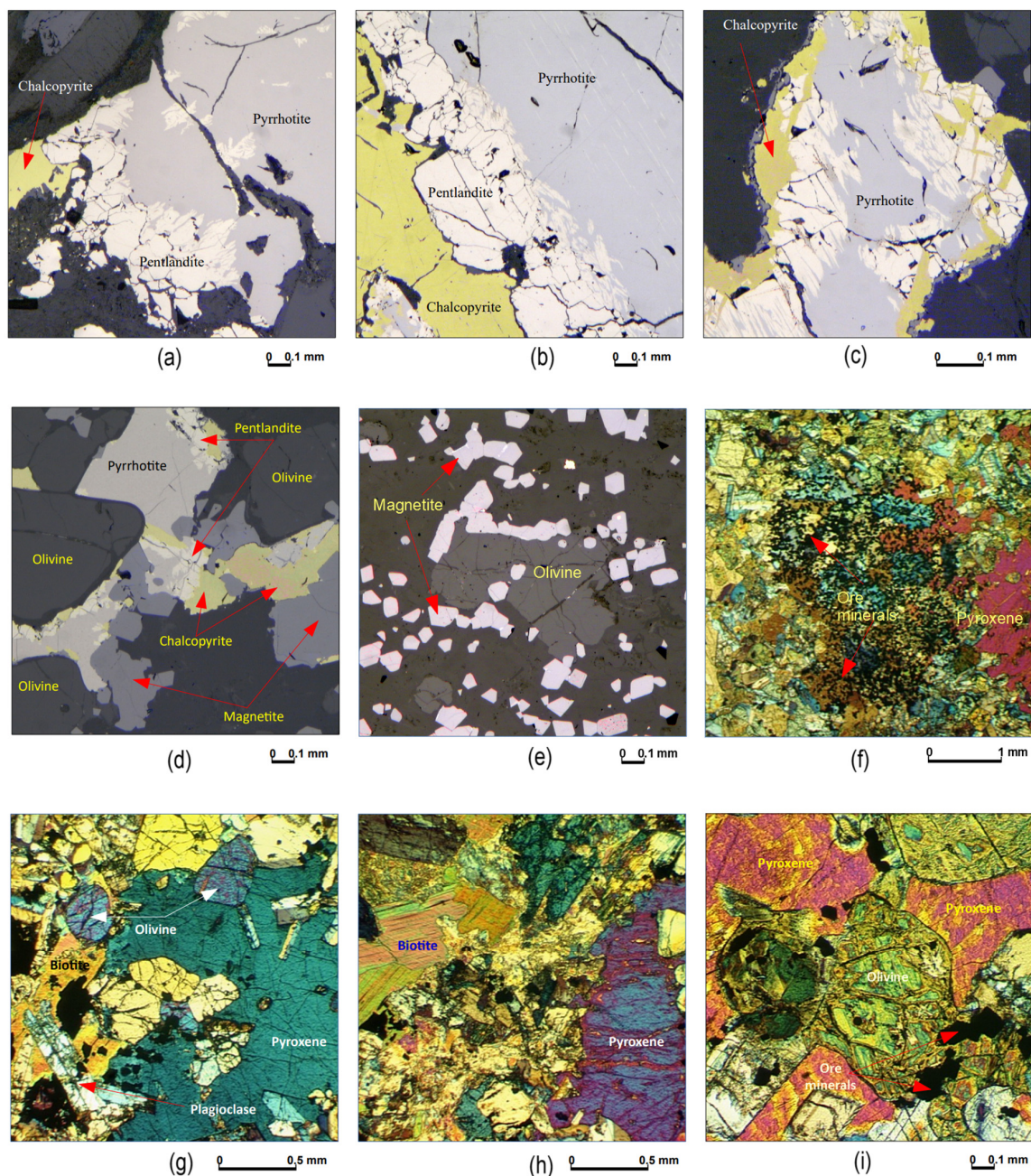


Figure 6. Microphotographs of thin sections from Ni-Cu Zapolyaroe ore deposit samples. (a) Intergrowth of pentlandite, pyrrhotite, and chalcopyrite crystals on the edges. Locally, pentlandite

is an aggregate (b) intergrowth between pentlandite, pyrrhotite, and chalcopyrite. The crystals of pentlandite are clearly fractured. (c) Chalcopyrite and pentlandite with exsolution texture. Phases are in contact with rock-forming minerals. (d) Olivine crystals in contact with ore minerals. Magnetite in contact with pyrrhotite and chalcopyrite. (e) Disseminated crystals of magnetite distributed in a scattered form. (f) Disseminated magnetite crystals (ore minerals). (g) Plagioclase laths with poikilitic texture. Olivine crystals are enclosed by the pyroxene oikocryst. (h) Biotite and main mineral phases. (i) Poikilitic pyroxene crystal with rounded olivine inclusions and plagioclase laths; iddingsite alteration in olivine is observed.

3.2. Point Load Strength Index

To evaluate the rock strength, 12 specimens were taken from the sampling area to carry out the Point Load Test. This number was relatively small because of the small amount of drill core sample material available. The Point Load Index of the Ni-Cu samples was $I_{S(50)} = 3.94 \pm 1.23$ MPa. In accordance with Equation (3), this corresponds to an average uniaxial rock compressive strength of $\sigma_D = 98.4$ MPa. According to the ISRM strength scale (Figure 7), the tested Zapolyarnoe samples were classified as rocks with high strength. The structural homogeneity, which is the variation in the coefficient in relation to middle size (σ/\bar{x}), was calculated to be 31.2% for the Zapolyarnoe specimens. This value was high, which meant that the irregular rock samples were heterogeneous and a larger sample would normally be recommended.

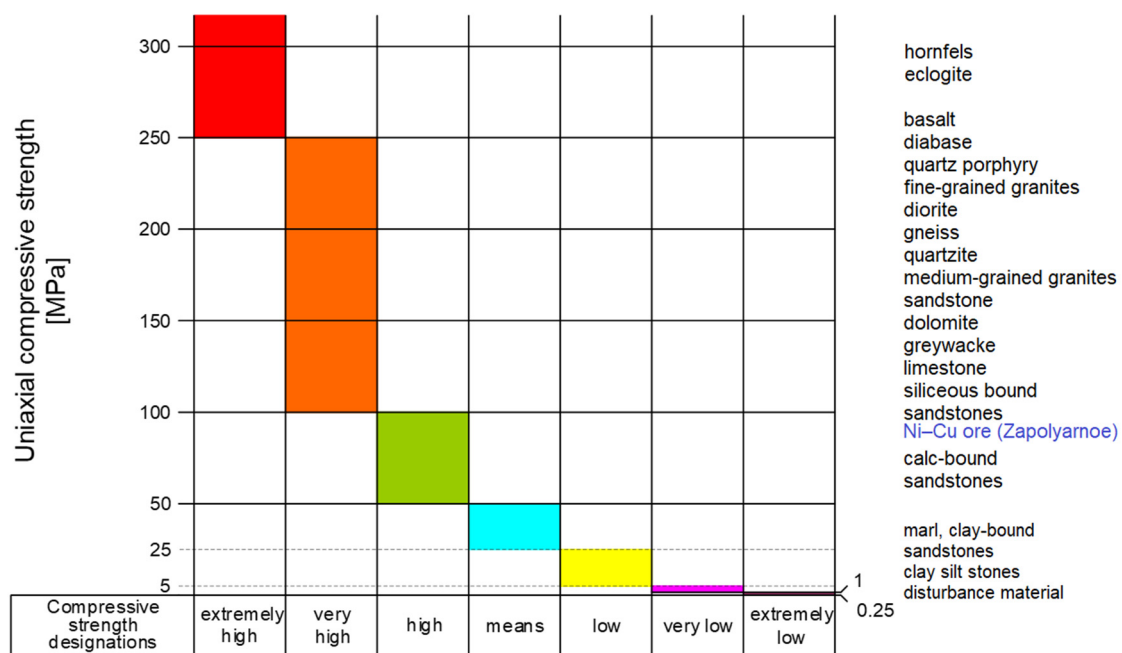


Figure 7. Data from commonly used descriptions for the uniaxial compressive strength of rocks [53] in accordance with the selected sample (Ni-Cu ore) highlighted.

3.3. Microindentations and Crack Morphology Results

Up to 50 microindentations were made for each of the mineral phases. The fracture toughness values and Vickers Hardness Numbers of the mineral phases were determined (Table 1). This study selected areas in the phases that purposely avoided pores and microfractures. The results for the Vickers Hardness (Figure 8) and fracture toughness (Figure 9) were plotted and compared. To avoid influences that could originate from the grain boundaries, these points were analysed separately.

Table 1. Vickers Hardness Number (VHN) in n/mm^2 and fracture toughness (K_{IC}) in $MN/m^{3/2}$ for each main phase.

Mineral Phase	VHN		K_{IC}	
	Mean	Stdev	Mean	Stdev
Pentlandite	254.91	2.95	1.59	0.33
Pyrrhotite	303.65	7.09	0.90	0.14
Chalcopyrite	211.22	7.91	0.63	0.16
Magnetite	866.35	80.84	1.63	0.62
Olivine	968.37	50.32	1.24	0.48
Feldspar	816.76	46.10	1.33	0.40

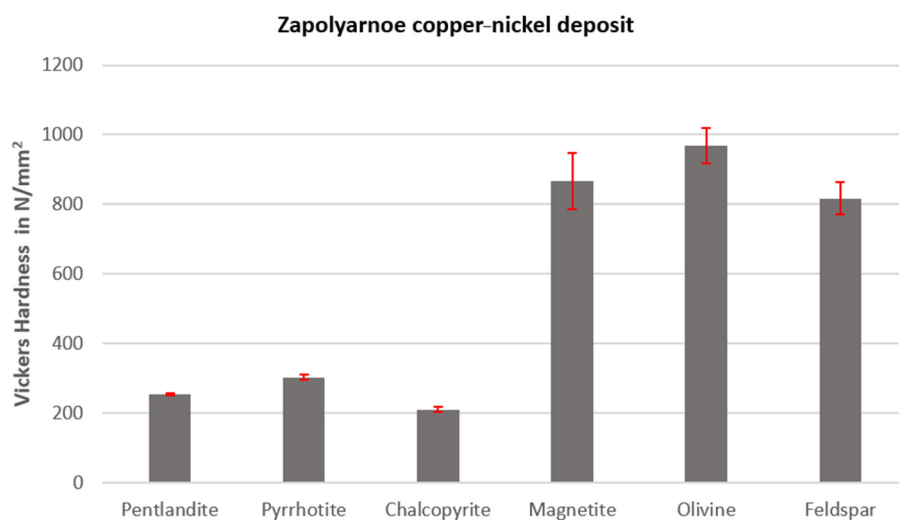


Figure 8. Vickers Hardness Number obtained for the main mineral phases in Zapolyarhoe.

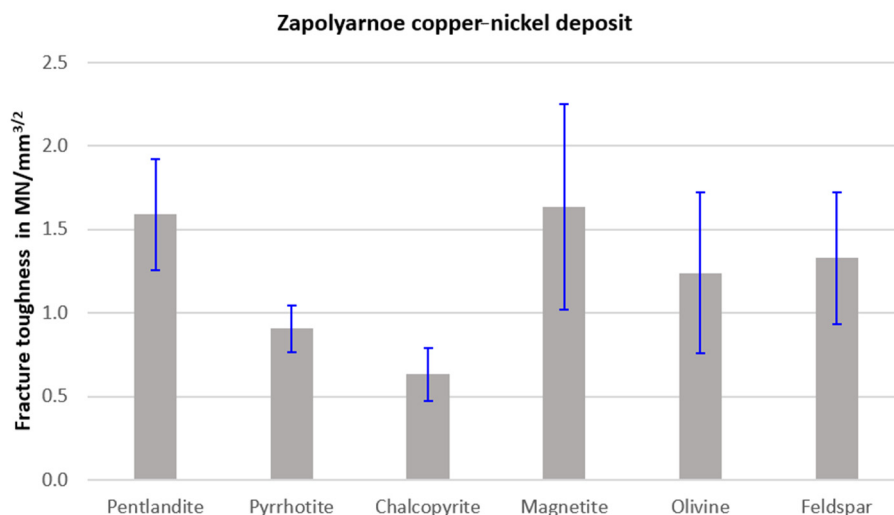


Figure 9. Fracture toughness values obtained for the main mineral phases from Zapolyarhoe.

The microindentations were carried out on a mesh of approximately 20 μm from an initial point close to the grain boundary (Figure 10a). The load was 245.2 mN for chalcopyrite, pentlandite, and pyrrhotite with a holding time of 15 s.

The same time was used for magnetite, olivine, and feldspar, but the load was raised to 490.3 mN. The reason for this is that these minerals have greater hardness, so the indentations resulting from this load were very small at the scale of observation that was used.

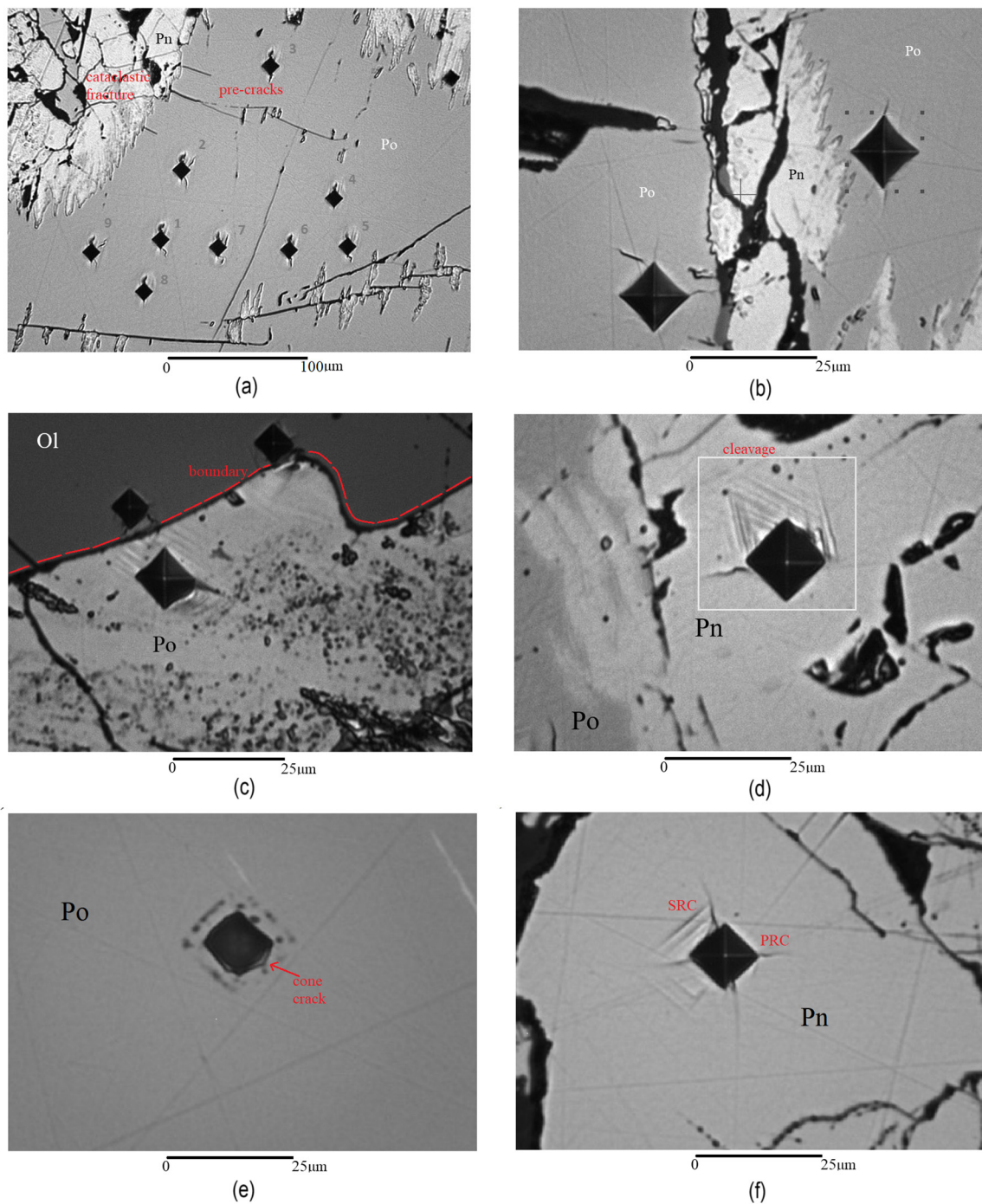


Figure 10. Vickers Hardness microindentation investigation. (a) Systematic analysis of a polished section, considering an equidistant mesh and avoiding irregularities (marks 1 to 9). (b) Example of microindentation close to a boundary. (c) Boundary between a rock-forming mineral (olivine) and an ore phase (pyrrhotite). (d) Lamination after indentation in pentlandite. (e) Cone crack observed after indentation in pyrrhotite. (f) Case IV according to morphology description (PRC + SRC) in pentlandite. (Pn) pentlandite; (Po) pyrrhotite; (Ol) olivine; (Cp) chalcopyrite.

Upon analysing the Vickers Hardness data, it is evident that the hardness values of ore minerals were often lower than those of rock-forming minerals, except for magnetite, which exhibited both high hardness and high fracture toughness. A significant chromium content (11.72% wt) explained this behaviour after indentation, as often no cracks occurred in magnetite. For pyrrhotite, only small cracks were observed (Figure 10a). Furthermore, a

cone crack was detected in pyrrhotite (Figure 10e). In chalcopyrite, crack propagation was evident in two directions (L_2 and L_3), but in the other two directions crack propagation was negligible (Figure 10e). Most of the crack morphologies for chalcopyrite were classified as PRCs. In the case of pentlandite, the mineral phase itself contained original cracks (Figure 10a,b). Owing to the presence of such irregularities in the mineral phase, the crack propagation showed no common pattern (Figure 10f). In the case of magnetite, it was common to observe cracks of the PRC + SRC type.

To provide a clearer visual representation of the predominant types of cracks formed during indentation, a comparative graphical analysis was conducted to examine the occurrence of primary radial cracks, secondary radial cracks, and other possible morphologies (Figure 11). Upon analysis, it was evident that pyrrhotite and chalcopyrite exhibited a generation of primary radial cracks (PRCs) or the absence of crack propagation (NC). Conversely, in pentlandite, the formation of secondary radial cracks (SRCs) was prevalent. Although SRC generation without the presence of PRCs was uncommon, this was attributed to the significant original cracks present in the pentlandite (Figure 10d).

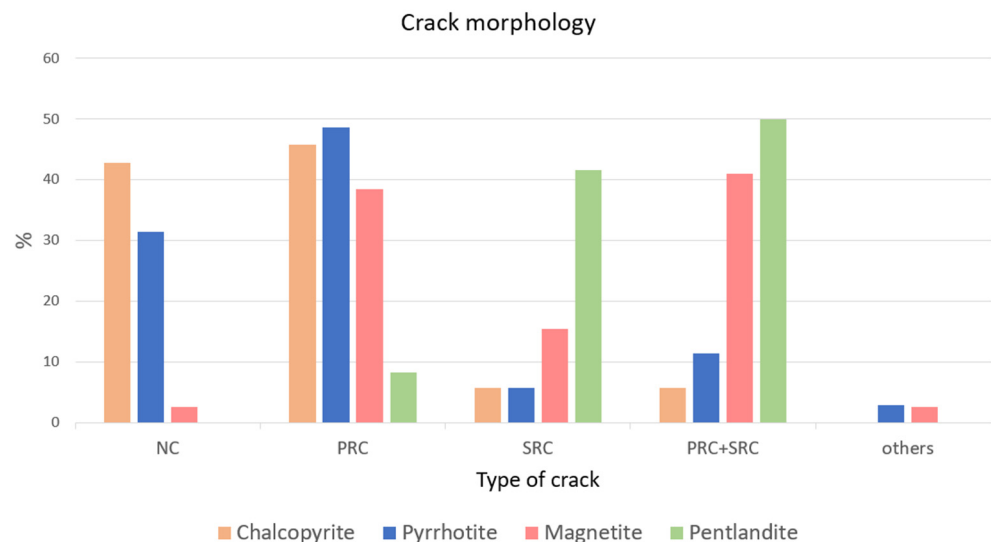


Figure 11. The percentage of cracks according to morphology: primary radial cracks (PRCs), secondary radial cracks (SRC), a combination of both (PRC + SRC), and other types of cracks (others) for the phases of chalcopyrite, pyrrhotite, magnetite, and pentlandite. The graphic also includes the percentage where no cracks (NC) were observed.

For the rock-forming minerals, olivine and feldspar, the microindentation showed a higher hardness value compared to the ore minerals. The response of olivine to microindentation was determined as a trend because primary radial cracks following the L_2 and the L_4 directions were generated in most of the tests. This fracture propagation was oriented towards the boundary (Figure 10c). Delamination textures were also visible in the case of pyrrhotite when indenting near the grain boundary with olivine (Figure 10c). In the case of magnetite studies, cracks were observed in many directions. In a few cases, a radial crack was found near the remaining indentation.

3.4. Mineral Liberation Analysis Results

An experimental study was conducted in the IART Institute facilities using a Single Toggle Jaw Crusher RETSCH model BB 250 XL (Retsch GmbH, Haan, Germany). Size reduction takes place in the wedge-shaped area between a fixed arm and one moved by an eccentric drive shaft. The elliptical motion crushes the sample which is moved towards the crushing gap under gravity. The potential of the jaw crusher was evaluated in terms of pre-concentration/selectivity after material size reduction with a compressive constant input gap of 30 mm.

This model of crusher is used for rapid and effective crushing and pre-crushing of materials. The input material was macroscopically described and weighed, resulting in an initial sample total of 2 kg (the particles after PLT are the feed material for Jaw Crusher). From the crushed product, the particle size distribution was obtained by sieving with apertures sizes of 2800, 1400, 710, 355, 180, and 125 μm . The sieving was performed using a Haver EML 200 sieve shaker (Retsch GmbH, Haan, Germany) for 10 min at a constant amplitude. The obtained fractions were analysed using Mineral Liberation Analysis (Figure 12) and the particle size distribution results of the combined data for all size fractions were plotted (Figure 13). The mass median diameter (D_{50}) was calculated to be 2.93 mm.

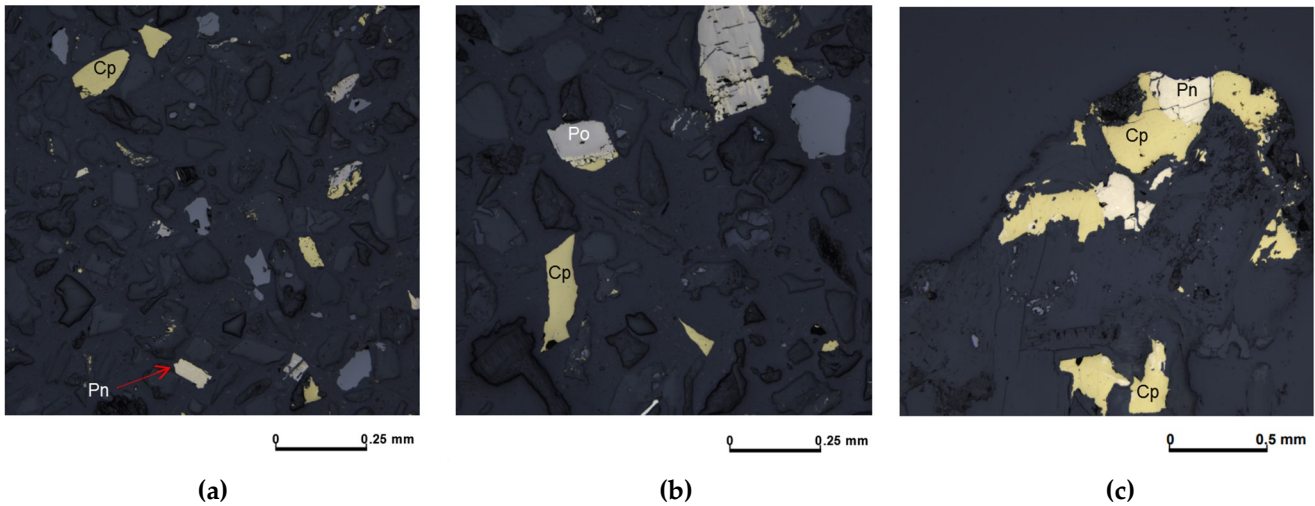


Figure 12. Microphotographs used as examples of liberated ore and non-liberated ore in different fractions. (a) Fraction 125/180 μm , (b) fraction 180/355 μm , and (c) fraction 1400/2800 μm . Cp: Chalcopyrite, Pn: Pentlandite, Po: Pyrrhotite.

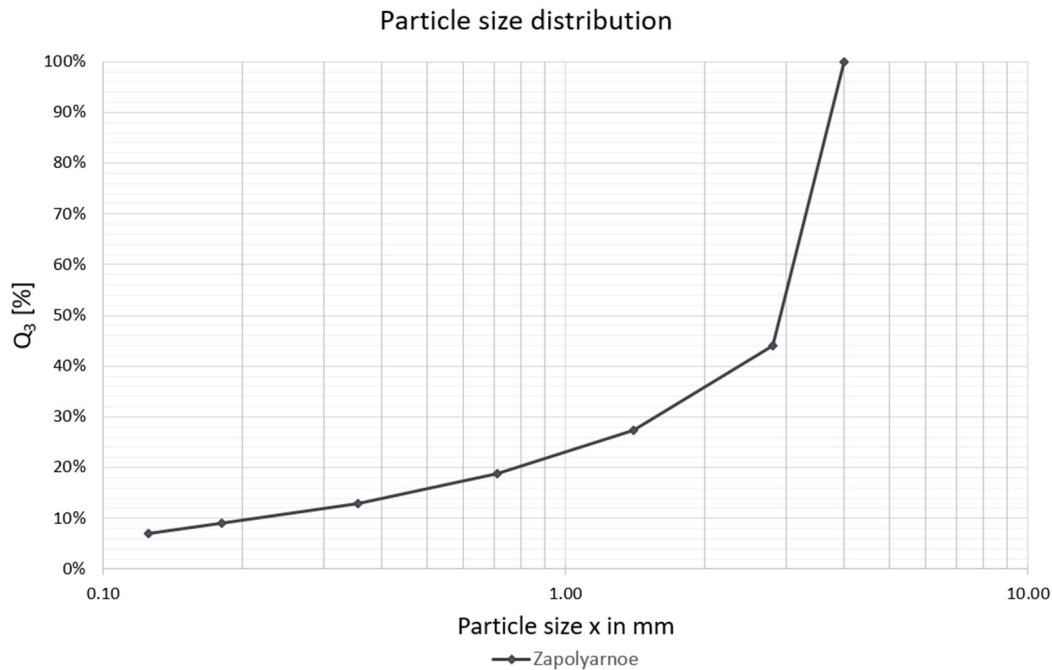


Figure 13. Particle size distribution for the crushed Ni-Cu ore from Zapolyarnee.

3.4.1. Mode Mineralogy Data

The modal composition of the feed material was determined based on the MLA results. Seventeen phases were identified (Figure 14). The mode mineralogy data obtained for the seven fractions were expressed in wt% for each mineral phase (Figure 15). Optical microscopic analysis of unprocessed materials revealed the prevalence of magnesium-rich forsterite olivine, feldspar, and chromium-rich magnetite phases. The forsterite exhibited its largest concentration in the portion larger than 2800 μm, with 48 wt%.

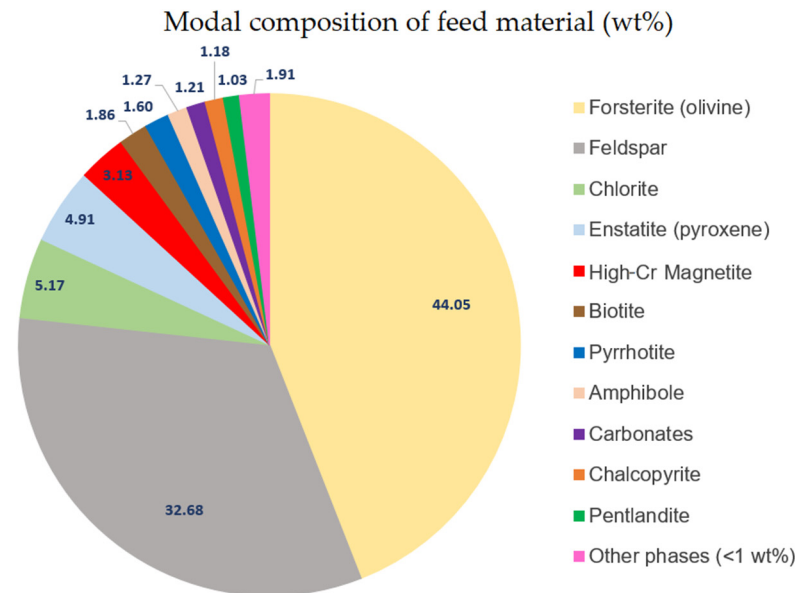


Figure 14. Modal composition (wt%) of the feed material calculated for the Ni-Cu samples. The phases included in the group below 1 wt% correspond to spinel (0.88 wt%), ilmenite (0.33 wt%), quartz (0.33 wt%), pyrite (0.25 wt%), apatite (0.10 wt%), and anhydrite (0.02 wt%).

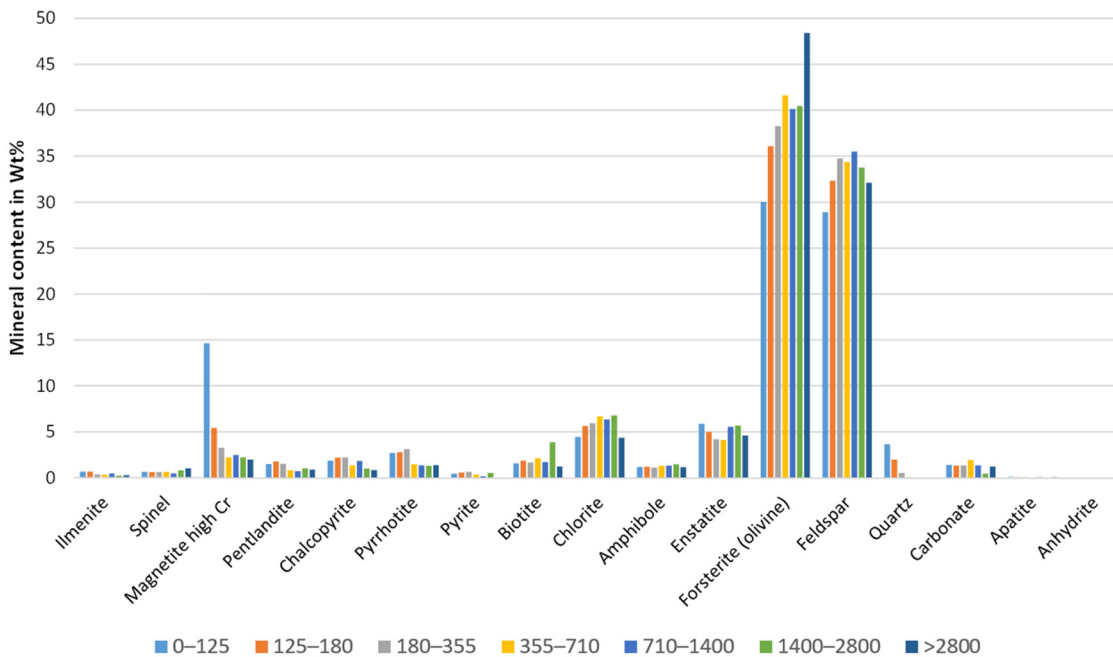


Figure 15. The mineral content of the product as a percentage identified via MLA for each size fraction (in μm) of the Zapolyarnoe samples.

The concentration of feldspar remained reasonably consistent across all fractions, with the variation ranging from 28 to 35 wt%. The results for pyroxene (enstatite), biotite, chlorite (secondary), amphibole, and carbonates remained steady and were consistently below 10 wt% for all fractions. Quartz was exclusively found in small particles. Concerning the ore minerals, magnetite exhibited an increase in weight percentage for smaller particle sizes (less than 125 μm), exceeding 14 wt%. The comparative graph (Figure 15) clearly shows an increase in the amount of chromium-rich magnetite. The abundant presence of magnetite in the smaller fractions was evident based on the mineral sizes identified under the microscope. It typically measured less than 0.4 mm, as previously mentioned in the thin-section descriptions.

3.4.2. Degree of Mineral Liberation

This section presents the data in terms of the liberation degrees obtained for magnetite, pyrrhotite, pentlandite, and chalcopyrite.

The degree of liberation was plotted as a function of the size fraction (in μm). Pentlandite was mainly associated with two or more phases (binary or ternary) in fractions larger than 125 μm , while at fractions up to 355 μm , pentlandite was practically not liberated (Figure 16a). Mineral locking showed that pentlandite was 43.4% liberated (for 0/125 μm particles), 8.7% locked (binary) to pyrrhotite, 3.9% locked (binary) to chalcopyrite, 2.4% locked (binary) to magnetite, and 13.8% locked (binary) to non-sulphide gangue (NSG). In the case of chalcopyrite, the degree was similar, although with higher liberation in fractions below 355 μm (Figure 16b). It was 50.1% liberated (for 0/125 μm particles), 3.1% locked (binary) to pyrrhotite, 3.7% locked (binary) to pentlandite, 2.6% locked (binary) to magnetite, and 17.2% locked (binary) to non-sulphide gangue.

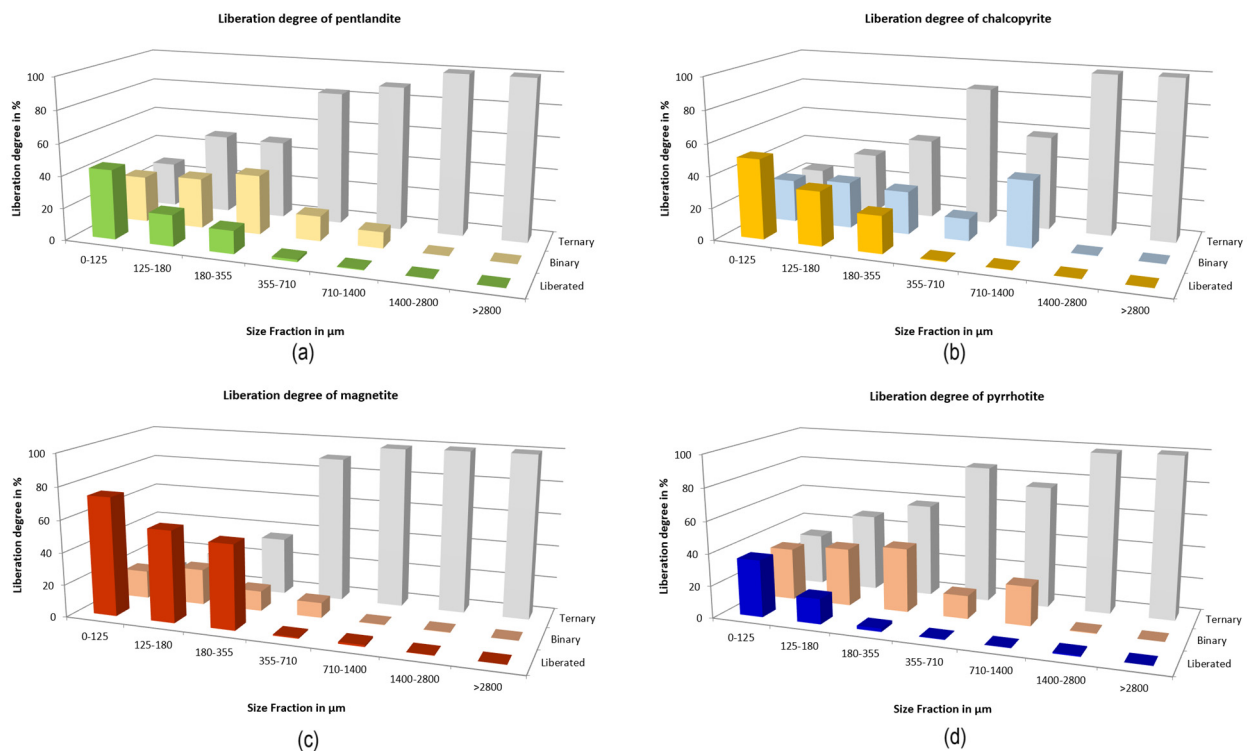


Figure 16. Liberation degree (based on 100% liberation) (a) pentlandite, (b) chalcopyrite, (c) magnetite, and (d) pyrrhotite.

In the case of magnetite, the fraction below 125 μm was 73.5% liberated, and just 17.35% was associated with other phases (binary). This increase was visible for fractions below 355 μm in contrast with coarse size classes, larger than 355 μm , where magnetite was associated generally with two phases (Figure 16c). The main phases locked with magnetite

were gangue minerals, representing 5.96% in 125/280 μm fractions, which decreased to 2.86% in fractions below 125 μm . Magnetite was also highly locked with pyrrhotite in the fraction below 125 μm (2.36%). For pyrrhotite, the liberation degree was lower than those of valuable minerals, at 35.55% in the fraction smaller than 125 μm (Figure 16d). An important relation in binary particles is the association with pentlandite, which reached 26.15% for the 180/355 μm fraction, decreased to 8.1% for the fraction below 125 μm .

4. Discussion

The evaluation of Ni-Cu samples from Zapolyarnoe in relation to the entire deposit becomes challenging when knowledge of the specific interval of the samples is absent and information on the spatial variation of the deposit is limited. The evaluation of resource estimation and reservoir modelling is not possible, as it is difficult to accurately model the geometry, continuity, and grade distribution of the reservoir without spatial data. Nevertheless, the comprehensive assessment of mineralogical and physical characteristics both before and after comminution has consistently yielded valuable findings for comprehending the material's behaviour and processing.

Upon examining thin sections, significant occurrences of grains with idioblastic textures were observed for rock-forming minerals such as olivine and pyroxene (Figure 6g). In contrast to the exsolution phases (pentlandite, chalcopyrite, and pyrrhotite), these rock-forming minerals show preferential breakage of the mineral aggregates along grain boundaries due to the distinct properties at the boundary contact. The differences include hardness and the sharp boundary contacts, in contrast to the intergrowth between pentlandite and pyrrhotite, for example. After comminution with a jaw crusher, grains containing binary or ternary locking remained in the case of the exsolution phases, mainly pentlandite, chalcopyrite, and pyrrhotite. The locking of exsolution phases after comminution was also evidenced by microindentation at the grain boundaries, where the trend showed that when indenting one of these phases the fracture did not propagate beyond the grain boundary and followed this direction, for example, olivine (Figure 10c).

The consideration of well-studied mineralogical properties is crucial to understanding the mechanical behaviour of minerals. Olivine, feldspar, and pyroxene exhibit remarkably high hardness values, in contrast to pentlandite, chalcopyrite, and pyrrhotite, which exhibit lower hardness values. On the other hand, magnetite shows a unique behaviour attributed to the presence of both primary and secondary radial cracks. These cracks contribute to its ability to separate from other phases and explain its high fracture toughness despite having a high Vickers Hardness Number. Unlike magnetite, chromium-rich minerals such as chromite tend to have lower fracture toughness.

A comparison can be made with pentlandite, as mentioned previously, which presents a higher fracture toughness value (Figure 9). This higher value despite low VHN could be due to the fact that grains of pentlandite have a large number of intrinsic fractures. Pre-existing microstructural defects in pentlandite were linked with an upsurge in the formation of secondary radial cracks observed during Vickers Hardness Testing. In addition, it was observed that chalcopyrite was generally found interfacing with harder minerals and bordering intergrowth. Pentlandite was found interlocking with pyrrhotite in most of the textural observations, explaining why chalcopyrite had a higher liberation degree, in contrast with pyrrhotite, which remained highly locked with pentlandite.

By comparing the degree of liberation with the mineral phase content per fraction (Figure 17a), the increase was accentuated in the fractions smaller than 355 μm , with a decrease between 355 and 710 μm in terms of the content observed for chalcopyrite. When comparing the phase contents of each fraction (Figure 18a–d), they did not vary significantly, except in the case of magnetite.

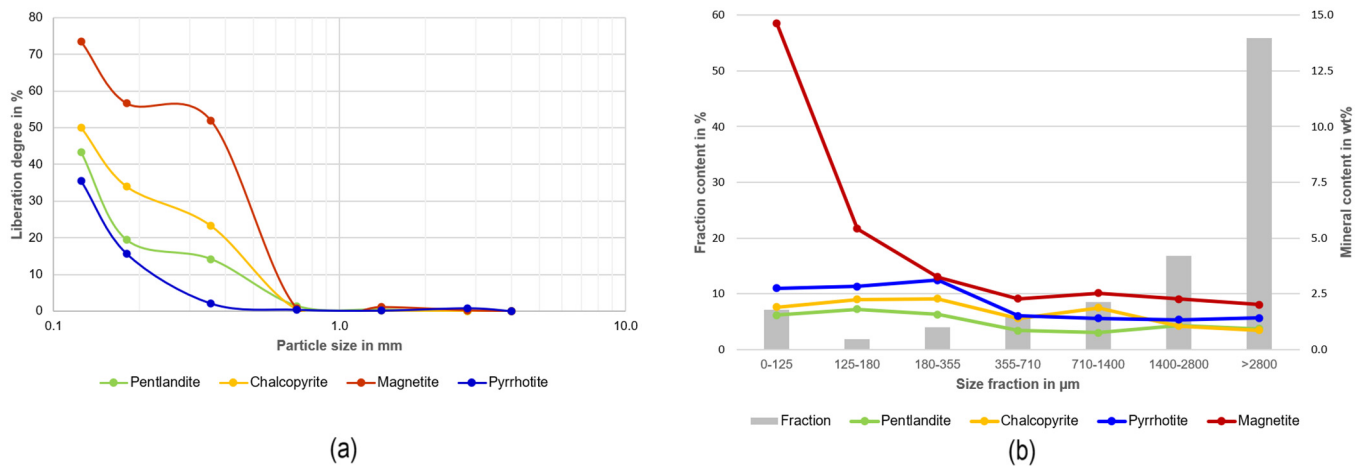


Figure 17. (a) Fraction content in percentages in relation to minerals of pentlandite, chalcopyrite, pyrrhotite, and magnetite. (b) Degree of liberation of pyrrhotite, pentlandite, chalcopyrite, and magnetite with respect to particle size.

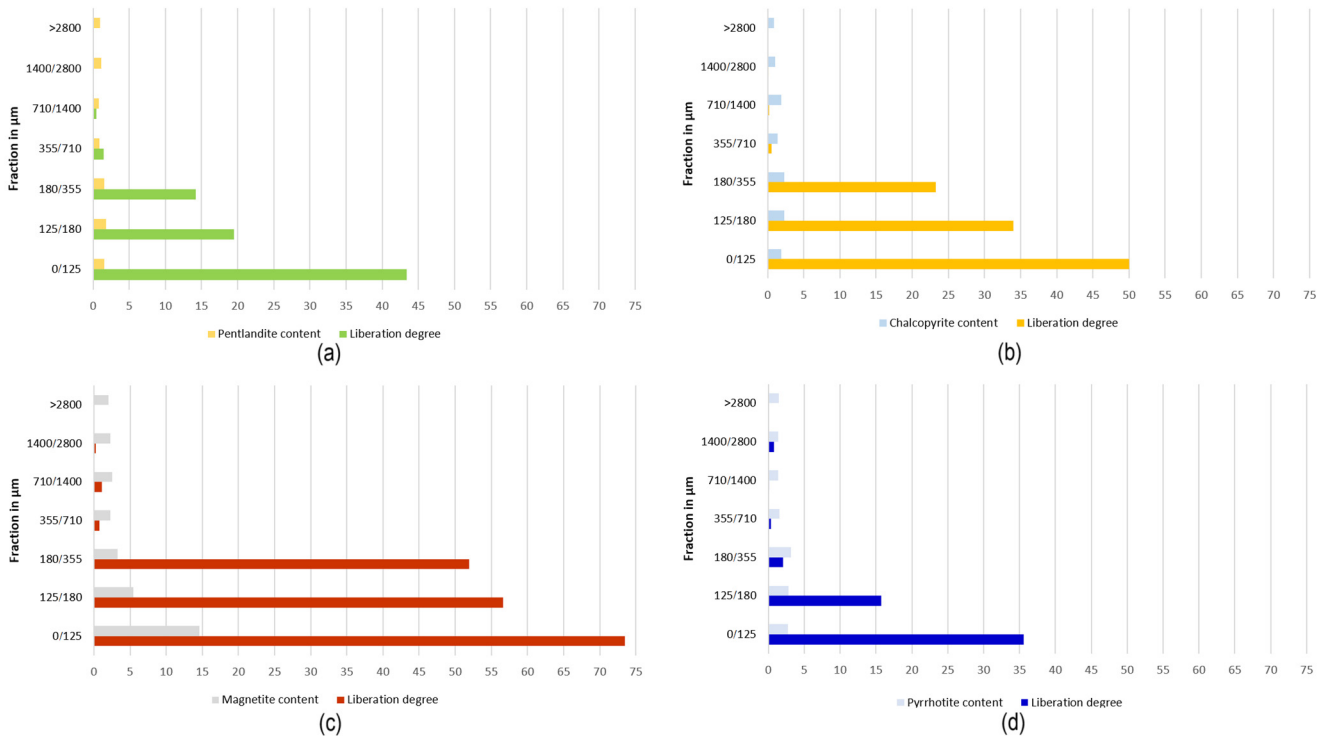


Figure 18. Comparison of liberation degree and mineral content of (a) pentlandite, (b) chalcopyrite, (c) magnetite, and (d) pyrrhotite.

When considering the degrees of liberation of pyrrhotite, pentlandite, chalcopyrite, and magnetite with respect to particle size, it can be seen that the chance to separate fully liberated magnetite is high in the small fraction (73.5% liberated) (Figure 17b). A separation possibility, due to the high liberation of magnetite, could be magnetic separation. Strongly magnetic minerals, such as magnetite, Fe-Ti oxides (ilmenite), and iron sulphides (pyrrhotite), can be removed from gangue via low-intensity magnetic separation [54–57]. Examples of magnetic separation tools include discs, drum and roll separators, and overhead magnets.

The investigations carried out on the Zapolyarnoe samples specifically addressed the topics of mineral liberation and preferential breakage in ore mineral processing. The

findings revealed that certain rock-forming minerals, such as olivine and pyroxene, possess characteristics that render them suitable for selective comminution at least when using compression stress from jaw crushers. Additionally, magnetite, due to its high fracture toughness, exhibits favourable properties for processing, particularly in coarser fractions (coarser than 355 μm) where full liberation is not achieved. In contrast, exsolution phases including pentlandite, chalcopyrite, and pyrrhotite demonstrate limited suitability for selective comminution. However, in accordance with expectations, the jaw crusher study confirmed increases in the grades of the key mineral phases (pentlandite and pyrrhotite) in the finer fractions, reaching values of 1.8 and 2.3 wt% respectively (Figure 17a).

In this study, a distinction was observed for the prevalent mineral found in copper–nickel deposits. While pyrrhotite is usually the predominant mineral or is found in a relatively similar ratio to magnetite (including Sudbury, Tati Phoenix, and Nkomati) [58–60], magnetite was found to be the most abundant mineral in this particular case.

Despite pyrrhotite exhibiting lower flotation activity compared to chalcopyrite and pentlandite, its high content in the ore poses challenges for selective flotation of minerals [58,59]. When pyrrhotite enters copper and nickel concentrates, it diminishes their quality, leading to significant difficulties in managing the excessive release of sulphur dioxide during the metallurgical process. By separating pyrrhotite into a distinct product, the quality of a nickel concentrate can be enhanced, and the burden on metallurgical processes can be reduced. In theory, it is possible to produce separate concentrates of nickel (pentlandite), copper (chalcopyrite), and iron. However, achieving a clean separation of pentlandite from pyrrhotite is challenging in practice. Utilising ferromagnetic properties or flotation, as described, appears to be the most practical option in this case.

This investigation emphasises the importance of considering the relationship between mineralogical parameters and physical properties when interpreting the enrichment of the ore. Physical observations such as mineral association, grain boundary characteristics, intrinsic fractures, and particle size are crucial to understanding the selectivity potential and product quality because they allow the correlation of textural parameters with expected behaviour and thereby reduce processes that require high energy intensity while seeking the best way to separate the desired phases. A jaw crusher is suitable for crushing material with different strengths quickly. An enrichment at 400 μm can be shown, although it cannot be determined whether the jaw crusher is the most suitable comminution machine to exploit the selectivity potential of the material.

5. Conclusions

The evaluation of Ni–Cu polymetallic ore samples obtained from drilling ore in Zapolyarnoe (Russia) provided the following findings:

- Even from a small amount of drill core material, valuable information for mineral processing can be derived;
- The results of this study demonstrate that certain mineral phases exhibit enrichment, which is related to the physical properties of the rock and grain boundary behaviour. The importance of considering the relationship between mineralogical parameters and physical properties when interpreting ore concentration is emphasised by this study;
- The degree of liberation generally exhibits variation in relation to particle size, where smaller fractions tend to have a greater likelihood of achieving complete liberation of magnetite and, to a lesser extent, chalcopyrite, pentlandite, and pyrrhotite;
- Certain rock-forming minerals, such as olivine and pyroxene, exhibit intrinsic features for preferential breakage, while exsolution phases such as pentlandite, chalcopyrite, and pyrrhotite demonstrate limited suitability;
- Magnetite was found with higher content than pyrrhotite in the copper–nickel ores from the Zapolyarnoe deposit in this case study, which differed from the common predominance of pyrrhotite in other classical Ni–Cu deposits, for example, Sudbury in Canada;

- The variation of pyrrhotite/magnetite poses challenges for flotation due to pyrrhotite’s negative impact on concentrate quality and sulphur dioxide emissions during the metallurgical process compared to magnetite. The high presence of chromium in magnetite explains the high value of fracture toughness;
- MLA demonstrated the efficient crushing of minerals with varying hardness values and accurate assessment of enrichment for Cu-Ni fractions below 400 µm. However, it should be noted that a jaw crusher may not be the optimal tool for evaluating selectivity potential due to the relatively small increases in the concentration of the target minerals;
- Further studies and alternative methods, such as utilising ferromagnetic properties or flotation, are recommended to achieve improved separation of pentlandite from pyrrhotite and to target magnetite as a potential mineral to maximise the enrichment after comminution.

Author Contributions: Conceptualisation, A.H.B., O.P. and H.L.; methodology, A.H.B. and O.P.; formal analysis, A.H.B. and O.P.; investigation, A.H.B.; writing—original draft preparation, A.H.B.; writing—review and editing, A.H.B., O.P. and H.L.; visualisation, A.H.B.; supervision, H.L. and O.P.; project administration, H.L.; funding acquisition, H.L. All authors have read and agreed to the published version of the manuscript.

Funding: This research is funded by the Deutsche Forschungsgemeinschaft (DFG, German Research Foundation), Grant No. 429570010.

Data Availability Statement: Data will be made available on request.

Acknowledgments: We thank our project partners at the Institute of Physical Chemistry and the Institute of Mineralogy at the TU Bergakademie Freiberg for their technical support and discussion.

Conflicts of Interest: The authors declare no conflicts of interest.

References

1. Norgate, T.; Jahanshahi, S. Low grade ores—Smelt, leach or concentrate? *Miner. Eng.* **2010**, *23*, 65–73. [[CrossRef](#)]
2. McLellan, B.C.; Yamasue, E.; Tezuka, T.; Corder, G.; Golev, A.; Giurco, D. Critical minerals and energy—impacts and limitations of moving to unconventional resources. *Resources* **2016**, *5*, 19. [[CrossRef](#)]
3. Aleksandrova, T.; Nikolaeva, N.; Afanasova, A.; Romashev, A.; Kuznetsov, V. Selective disintegration justification based on the mineralogical and technological features of the polymetallic ores. *Minerals* **2021**, *11*, 851. [[CrossRef](#)]
4. Nkuna, R.; Ijoma, G.N.; Matambo, T.S.; Chimwani, N. Accessing Metals from Low-Grade Ores and the Environmental Impact Considerations: A Review of the Perspectives of Conventional versus Bioleaching Strategies. *Minerals* **2022**, *12*, 506. [[CrossRef](#)]
5. Saramak, D. Challenges in raw material treatment at the mechanical processing stage. *Minerals* **2021**, *11*, 940. [[CrossRef](#)]
6. Aleksandrova, T.; Nikolaeva, N.; Afanasova, A.; Romashev, A.; Kuznetsov, V. Justification for criteria for evaluating activation and destruction processes of complex ores. *Minerals* **2023**, *13*, 684. [[CrossRef](#)]
7. Tromans, D. Mineral comminution: Energy efficiency considerations. *Miner. Eng.* **2008**, *21*, 613–620. [[CrossRef](#)]
8. Ballantyne, G.R.; Powell, M.S. Benchmarking comminution energy consumption for the processing of copper and gold ores. *Miner. Eng.* **2014**, *65*, 109–114. [[CrossRef](#)]
9. Powell, M.S.; Morrison, R.D. The future of comminution modelling. *Int. J. Miner. Process.* **2007**, *84*, 228–239. [[CrossRef](#)]
10. Jeswiet, J.; Szekeres, A. Energy Consumption in Mining Comminution. *Procedia CIRP* **2016**, *48*, 140–145. [[CrossRef](#)]
11. Kukolj, I.; Iravani, A.; Ouchterlony, F. Using Small-scale Blast Tests and Numerical Modelling to Trace the Origin of Fines Generated in Blasting. *BHM Berg-Und Hüttenmänn. Monatshefte* **2018**, *163*, 427–436. [[CrossRef](#)] [[PubMed](#)]
12. Vizcarra, T.G.; Wightman, E.M.; Johnson, N.W.; Manlapig, E.V. The effect of breakage mechanism on the mineral liberation properties of sulphide ores. *Miner. Eng.* **2010**, *23*, 374–382. [[CrossRef](#)]
13. Sandmann, D.; Gutzmer, J. Use of Mineral Liberation Analysis (MLA) in the Characterization of Lithium-Bearing Micas. *J. Miner. Mater. Charact. Eng.* **2013**, *1*, 285–292. [[CrossRef](#)]
14. Lieberwirth, H. Securing resources for growth—Challenges and opportunities for comminution in mineral processing. In *Proceeding of the Conference in Minerals Engineering—Konferens i Mineralteknik*, Luleå, Sweden, 7–8 February 2017.
15. King, R.P. Comminution and liberation of minerals. *Miner. Eng.* **1994**, *7*, 129–140. [[CrossRef](#)]
16. King, R.P.; Schneider, C.L. Mineral liberation and the batch comminution equation. *Miner. Eng.* **1998**, *11*, 1143–1160. [[CrossRef](#)]
17. Hosten, C.; Cimilli, H. The effects of feed size distribution on confined-bed comminution of quartz and calcite in piston-die press. *Int. J. Miner. Process.* **2009**, *91*, 81–87. [[CrossRef](#)]

18. Klichowicz, M.; Lieberwirth, H. Modeling of realistic microstructures as key factor for comminution simulations. In Proceedings of the IMPC 2016—28th International Mineral Processing Congress, Québec City, QC, Canada, 11–15 September 2016.
19. Hesse, M.; Popov, O.; Lieberwirth, H. Increasing efficiency by selective comminution. *Miner. Eng.* **2017**, *103–104*, 112–126. [[CrossRef](#)]
20. Weng, X.; Li, H.; Song, S.; Liu, Y. Reducing the entrainment of gangue fines in low grade microcrystalline graphite ore flotation using multi-stage grinding-flotation process. *Minerals* **2016**, *7*, 38. [[CrossRef](#)]
21. Lois-Morales, P.; Evans, C.; Weatherley, D. Characterising tensile strength and elastic moduli of altered igneous rocks at comminution scale using the short impact load cell. *Powder Technol.* **2021**, *388*, 343–356. [[CrossRef](#)]
22. Lieberwirth, H.; Kühnel, L. Particle size effects on selectivity in confined bed comminution. *Minerals* **2021**, *11*, 342. [[CrossRef](#)]
23. Djordjevic, N. Image based modeling of rock fragmentation. *Miner. Eng.* **2013**, *46–47*, 68–75. [[CrossRef](#)]
24. Popov, O.; Lieberwirth, H.; Folgner, T. Quantitative charakterisierung der festgesteine zur prognostizierung des gesteineinflusses auf relevante produkteigenschaften und systemkenngrößen. teil 1: Anwendung der quantitativen gefügeanalyse. *AT Miner. Process* **2014**, *7–8*, 76–88.
25. Evans, C.L.; Wightman, E.M.; Yuan, X. Quantifying mineral grain size distributions for process modelling using X-ray microtomography. *Miner. Eng.* **2015**, *82*, 78–83. [[CrossRef](#)]
26. Mariano, R.A.; Evans, C.L. The effect of breakage energies on the mineral liberation properties of ores. *Miner. Eng.* **2018**, *126*, 184–193. [[CrossRef](#)]
27. Chen, K.; Yin, W. Investigation of liberation properties and mineral fracture mechanisms of iron ores with different mineral grain sizes at different grinding degrees. *Miner. Process. Extr. Metall. Rev.* **2023**, *40*, 2495–2504. [[CrossRef](#)]
28. Tolstykh, N.; Brovchenko, V.; Rad'ko, V.; Shapovalova, M.; Abramova, V.; Garcia, J. Rh, Ir, and Ru Partitioning in the Cu-Poor IPGE Massive Ores, Talnakh Intrusion, Skalisty Mine, Russia. *Minerals* **2022**, *12*, 18. [[CrossRef](#)]
29. Tolstykh, N.; Shvedov, G.; Polonyankin, A.; Korolyuk, V. Geochemical features and mineral associations of differentiated rocks of the norilsk 1 intrusion. *Minerals* **2020**, *10*, 688. [[CrossRef](#)]
30. Kalinin, A.A.; Kazanov, O.V.; Bezrukov, V.I.; Prokofiev, V.Y. Gold prospects in the western segment of the russian arctic: Regional metallogeny and distribution of mineralization. *Minerals* **2019**, *9*, 137. [[CrossRef](#)]
31. Yakubchuk, A.; Nikishin, A. Noril'sk-Talnakh Cu-Ni-PGE deposits: A revised tectonic model. *Miner. Depos.* **2004**, *39*, 125–142. [[CrossRef](#)]
32. Lightfoot, P.C. Advances in Ni-Cu-PGE Sulphide Deposit Models and Implications for Exploration Technologies. In Proceedings of the Fifth Decennial International Conference on Ore Deposits and Exploration Technology, Toronto, ON, Canada, 9–12 September 2007; pp. 629–646.
33. Starostin, V.I.; Sorokhtin, O.G. A new interpretation for the origin of the Norilsk type PGE-Cu-Ni sulfide deposits. *Geosci. Front.* **2011**, *2*, 583–591. [[CrossRef](#)]
34. Broch, E.; Franklin, J.A. The point-load strength test. *Int. J. Rock Mech. Min. Sci. Geomech. Abstr.* **1972**, *9*, 669–676. [[CrossRef](#)]
35. Brook, N. The equivalent core diameter method of size and shape correction in point load testing. *Int. J. Rock Mech. Min. Sci. Geomech. Abstr.* **1985**, *22*, 61–70. [[CrossRef](#)]
36. International Society for Rock Mechanics (ISRM); Commission on Testing Method; Working Group on Revision of the Point Load Test Method. Suggested method for determining point load strength. *Int. J. Rock Mech. Min. Sci. Geomech. Abstr.* **1985**, *22*, 51–60. [[CrossRef](#)]
37. Duryagina, A.; Talovina, I.; Shtyryaeva, A.; Popov, O. Application of Computer X-ray Microtomography for Study of Technological Properties of Rocks. *Key Eng. Mater.* **2018**, *769*, 220–226. [[CrossRef](#)]
38. Thuro, K. Bohrbarkeit beim konventionellen Sprengvortrieb. In *Münchener Geologische Hefte Reihe B: Angewandte Geologie*; Publisher: Munich, Germany, 1996; p. 149.
39. Raaz, V. Charakterisierung der Gesteinsfestigkeit mit Hilfe eines modifizierten Punktlastversuches. *Z. Geol. Wiss.* **2002**, *30*, 213–226.
40. Chau, K.T.; Wong, R.H. Uniaxial compressive strength and point load strength of rocks. *Int. J. Rock Mech. Min. Sci. Geomech. Abstr.* **1996**, *33*, 183–188. [[CrossRef](#)]
41. Alitalesh, M.; Mollaali, M.; Yazdani, M. Correlation between uniaxial strength and point load index of rocks. *Jpn. Geotech. Soc. Spec. Publ.* **2015**, *2*, 504–507. [[CrossRef](#)]
42. ISO 6507-1; Metallic Materials—Vickers Hardness Test—Part 1: Test Method. Standard International Organization for Standardization: Geneva, Switzerland, 2005.
43. Bravo, A.H.; Popov, O.; Lieberwirth, H. Mineralogical and micromechanical characterization of slags: Investigated on the example of a MnSiFe slag from electric arc furnace. *Min. Rep. Gluckauf.* **2021**, *157*, 546–559.
44. Tabor, D. The physical meaning of indentation and scratch hardness. *Br. J. Appl. Phys.* **1956**, *7*, 159–166. [[CrossRef](#)]
45. Rios, C.T.; Coelho, A.A.; Batista, W.W.; Gonçalves, M.C.; Caram, R. ISE and fracture toughness evaluation by Vickers hardness testing of an Al3Nb-Nb2Al-AlNbNi in situ composite. *J. Alloys Compd.* **2009**, *472*, 65–70. [[CrossRef](#)]
46. Blumenauer, H.; Pusch, G. *Technische Bruchmechanik*; Deutscher Verlag für Grundstoffindustrie: Leipzig, Germany, 1993.
47. Evans, A.G.; Charles, E.A. Fracture toughness determinations by indentation. *J. Am. Ceram. Soc.* **1976**, *59*, 371–372. [[CrossRef](#)]
48. Tanaka, K. Elastic/plastic indentation hardness and indentation fracture toughness: The inclusion core model. *J. Mater. Sci.* **1987**, *22*, 1501–1508. [[CrossRef](#)]

49. Gottlieb, P.; Wilkie, G.; Sutherland, D.; Ho-Tun, E.; Suthers, S.; Perera, K.; Jenkins, B.; Spencer, S.; Butcher, A.; Rayner, J. Using quantitative electron microscopy for process mineralogy applications. *JOM* **2000**, *52*, 24–25. [[CrossRef](#)]
50. Gu, Y. Automated Scanning Electron Microscope Based Mineral Liberation Analysis. An introduction to JKMRC/FEI Mineral Liberation Analyser. *J. Miner. Mater. Charact. Eng.* **2003**, *2*, 33–41. [[CrossRef](#)]
51. Schulz, B.; Merker, G.; Gutzmer, J. Automated SEM mineral liberation analysis (MLA) with generically labelled EDX spectra in the mineral processing of rare earth element ores. *Minerals* **2019**, *9*, 527. [[CrossRef](#)]
52. Spencer, S.; Sutherland, D. Stereological Correction of Mineral Liberation Grade Distributions Estimated By Single Sectioning of Particles. *Image Anal. Stereol.* **2000**, *19*, 175–182. [[CrossRef](#)]
53. International Society for Rock Mechanics (ISRM); Commission on Standardization of Laboratory and Field Tests. Suggested methods for determining the uniaxial compressive strength and deformability of rock materials. *Int. J. Rock Mech. Min. Sci. Geomech. Abstr.* **1978**, *16*, 138–140.
54. Svoboda, J. *Magnetic Methods for the Treatment of Minerals*; Elsevier: Amsterdam, The Netherlands, 1987; p. 50.
55. Svoboda, J.; Fujita, T. Recent Developments in Magnetic Methods of material separation. *Miner. Eng.* **2003**, *16*, 785–792. [[CrossRef](#)]
56. Tripathy, S.K.; Banerjee, P.K.; Suresh, N. Magnetic separation studies on ferruginous chromite fine to enhance Cr:Fe ratio. *Int. J. Miner. Metall. Mater.* **2015**, *22*, 217. [[CrossRef](#)]
57. Kumar, D.R.; Srinivas, R.D.; Sita Ram, R.P. Magnetic separation studies for a low grade siliceous iron ore sample. *Int. J. Min. Sci. Technol.* **2013**, *23*, 1–5. [[CrossRef](#)]
58. Becker, M.; de Villiers, J.; Bradshaw, D. The flotation of magnetic and non-magnetic pyrrhotite from selected nickel ore deposits. *Miner. Eng.* **2010**, *23*, 1045–1052. [[CrossRef](#)]
59. Xu, M.; Wilson, S. Investigation of seasonal metallurgical shift at Inco's Clarabelle mill. *Miner. Eng.* **2000**, *13*, 1207–1218. [[CrossRef](#)]
60. Boutroy, E.; Dare, S.A.S.; Beaudoin, G.; Barnes, S.-J.; Lightfoot, P.C. Magnetite composition in Ni-Cu-PGE deposits worldwide: Application to mineral exploration. *J. Geochem. Explor.* **2014**, *145*, 64–81. [[CrossRef](#)]

Disclaimer/Publisher's Note: The statements, opinions and data contained in all publications are solely those of the individual author(s) and contributor(s) and not of MDPI and/or the editor(s). MDPI and/or the editor(s) disclaim responsibility for any injury to people or property resulting from any ideas, methods, instructions or products referred to in the content.